Current Applied Physics xxx (xxxx) xxx–xxx

Contents lists available at ScienceDirect

Current Applied Physics

journal homepage: www.elsevier.com/locate/cap

Damping and transformation behaviors of $Ti_{50}(Pd_{50-x}Cr_x)$ shape memory alloys with x ranging from 4.0 to 5.0

Deqing Xue[a], Ruihao Yuan[a], Dezhen Xue[a], Yumei Zhou[a,*], Guojun Zhang[b], Xiangdong Ding[a], Jun Sun[a]

[a] State Key Laboratory for Mechanical Behavior of Materials, Xi'an Jiaotong University, Xi'an 710049, China
[b] School of Materials Science and Engineering, Xi'an University of Technology, Xi'an 710048, China

ARTICLE INFO

Keywords:
Shape memory alloy
Martensitic phase transformation
Damping
Dynamic mechanical analysis

ABSTRACT

The damping and transformation behaviors of $Ti_{50}(Pd_{50-x}Cr_x)$ shape memory alloys with x ranging from 4.0 to 5.0 are systematically investigated. The damping capacity (Q^{-1}) at the martensitic transformation is found to be inversely proportional to the square root of frequency, *i.e.,* $Q^{-1} \propto \omega^{-0.5}$. A relaxation peak or shoulder is observed slightly below the martensitic transformation damping peak for compositions within the compositional crossover region ($4.5 \leqslant x \leqslant 4.8$). Furthermore, the damping capacity at the martensitic transformation is smaller within the compositional crossover region ($4.5 \leqslant x \leqslant 4.8$), compared with that of compositions at both sides ($x = 4.0$ and $x = 5.0$). These observations can be ascribed to the hysteretic motion of interfaces between different phases near the compositional crossover region.

1. Introduction

The damping capacity (Q^{-1}) represents the capacity of a material to convert the mechanical energy of vibration into heat [1–3]. To reduce the noise/vibration or absorb shock/impact, materials with high damping capacity are attracting much attention nowadays [4–9]. Shape memory alloys (SMAs) have been considered as promising candidates as they possess both high damping capacities and good mechanical properties [10,11].

It is known that SMAs undergo a reversible martensitic transformation between high-symmetry austenite (A) and low symmetry martensite (M) in response to the change in temperature or stress field [11]. As a result of the martensitic transformation, two types of internal planar interfaces exist in SMAs, including the phase front between A and M phases, and the twin boundaries between two different martensite variants [11]. The hysteretic motion of these planar interfaces always dissipates energy, giving rise to the high damping capacity in SMAs [12,13]. The damping source associated with the A/M phase front occurs during martensitic transformation [12–14]. The A/M interface is generally mobile but strongly dissipative, resulting in a high damping peak at the transformation temperature [12–14]. But such a damping peak depends sensitively on thermal gradients (i.e., its damping value drops considerably when the temperature is fixed) and thus is a "transient peak" [12,14]. The other damping source appears in the martensite and is associated with the stress driven motion of twin boundaries. Extrinsic defects (*e.g.* hydrogen), or intrinsic microstructure components (*e.g.* the twin junctions) interact with twin boundaries via. either pinning/de-pinning [15,16] or jamming [17], and consequently lead to the dissipation of the mechanical energy. It is usually manifested as a "broad relaxation peak" after the martensitic transformation where martensite twins exist [6,18,19].

The twin boundary correlated damping capacity is thermal hysteresis free and independent on cooling/heating rate, thus is practically more applicable [6,8]. It has been shown that TiPd-based SMAs exhibit a "broad relaxation peak" or a high damping plateau within the ambient temperature range and could be good candidates for high damping materials [6,7,21]. The TiPd-based alloys is superior to TiNi-based alloy in the aspects of higher martensitic transformation temperature and larger size of twining shear [7]. Recently, a small thermal hysteresis ΔT was achieved in the compositional crossover region in $Ti_{50}(Pd_{50-x}Cr_x)$ between two different martensitic transformations, as indicated by the solid circle in Fig. 1 (a) [20,22]. The two different martensitic transformations have opposite changes in electrical resistance at the transformation temperature [22]. The possible underlying reason for the small ΔT is ascribed to the small interfacial strain at the austenite/martensite interface accommodated via coexistence of B19 and 9 R martensites [22]. As damping capacity is closely related with the hysteretic motion of interfaces, it is then of interest to explore the damping behaviors at such a compositional crossover region.

In the present study, we thus systematically investigated the

* Corresponding author.
E-mail address: zhouyumei@mail.xjtu.edu.cn (Y. Zhou).

https://doi.org/10.1016/j.cap.2018.03.025
Received 6 February 2018; Received in revised form 22 March 2018; Accepted 30 March 2018

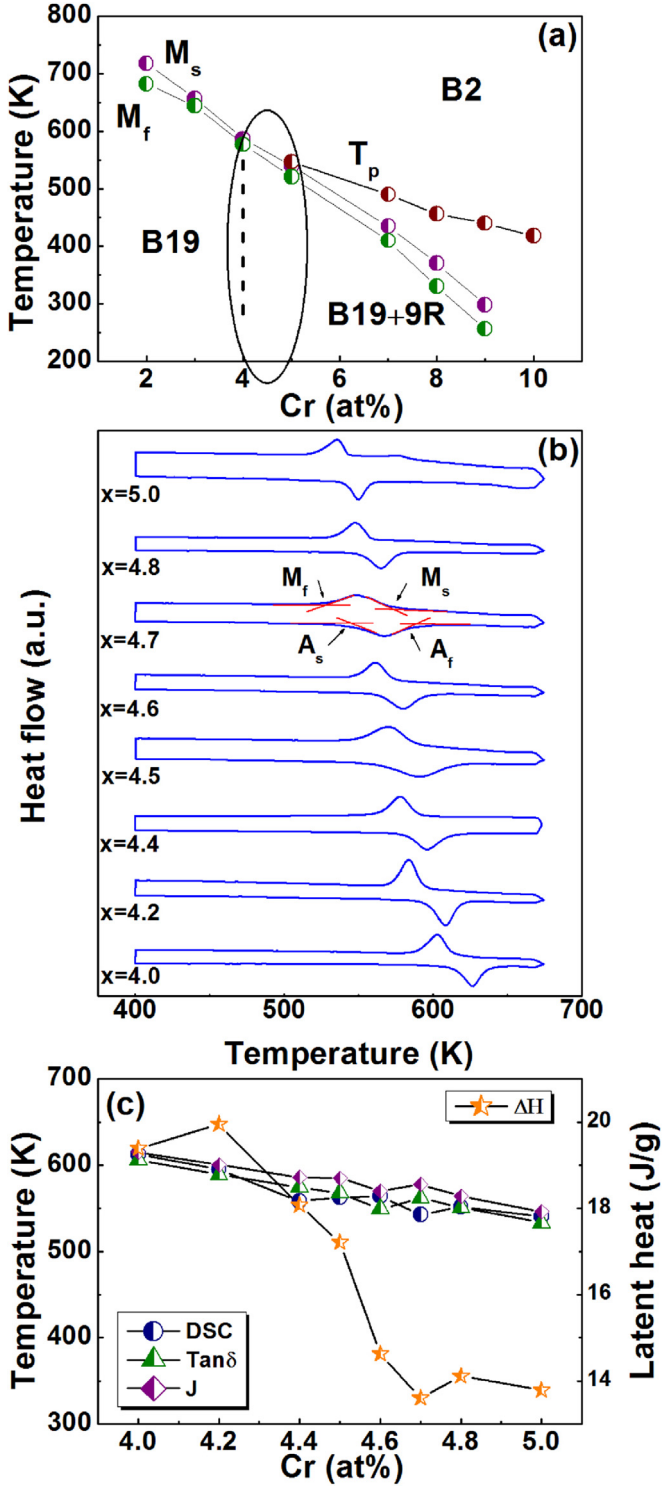

Fig. 1. (a) Phase diagram of $Ti_{50}(Pd_{50-x}Cr_x)$, after Enami et al. [20], with permission from publisher: ISIJ. M_s and M_f are the martensitic transformation start and finish temperatures, respectively. T_p is the temperature at which ER anomaly begins, defined in Ref. [20]. The solid circle indicates a crossover composition region, where the change in electrical resistance at the transformation temperature becomes opposite. (b) DSC results of $Ti_{50}(Pd_{50-x}Cr_x)$ SMAs with x ranging from 4.0 to 5.0. Arrows indicate the M_s. (c) The M_s temperatures determined by DSC measurement, damping capacity ($\tan\delta$) and storage compliance (J) are plotted as a function of Cr concentration x. Moreover, the latent heat ΔH during martensitic transformation as a function of Cr concentration x is shown as well.

damping capacity and phase transformation behaviors of $Ti_{50}(Pd_{50-x}Cr_x)$ alloys with x ranging from 4.0 to 5.0 by differential scanning calorimeter (DSC) and dynamic mechanical analysis (DMA). The results show that the damping capacity at the martensitic transformation is inversely proportional to the square root of frequency ($Q^{-1} \propto \omega^{-0.5}$). There exists a relaxation peak or shoulder slightly below the martensitic transformation damping peak within the compositional crossover region ($4.5 \leqslant x \leqslant 4.8$). Furthermore, the damping capacity of martensitic transformation is found to be smaller within the compositional crossover region ($4.5 \leqslant x \leqslant 4.8$) than that of compositions at both sides ($x = 4.0$ and $x = 5.0$). These observations can be ascribed to the hysteretic motion of interfaces between different phases near the compositional crossover region.

2. Experiment

Samples of $Ti_{50}(Pd_{50-x}Cr_x)$ (x = 4.0, 4.2, 4.4, 4.5, 4.6, 4.7, 4.8, 5.0 *at%*) alloys were prepared by arc melting a mixture of high purity metals (99.9% Ti, 99.9% Pd and 99.9% Cr) in an argon atmosphere. All the ingots were hot rolled to 1 mm thick. The specimens were then spark cut into suitable shapes for different experiments ($3 \times 3 \times 1$ mm^3 for DSC and $20 \times 2 \times 1$ mm^3 for DMA). They were then solution treated at 1273 K for 1 h in evacuated quartz tubes and quenched into ice water. In order to remove the affected surface layer, the specimens were mechanically polished.

DSC measurements were performed with a cooling/heating rate of 10 K/min between 400 K and 670 K to probe the martensitic transformation behaviors by exothermal/endothermic peaks. The damping properties (Q^{-1} or $\tan\delta$) and the anelastic storage compliance (J) were obtained by DMA using the single cantilever mode with displacement amplitude of 15 μm, i.e., one end was fixed and stress field with sinusoid period (AC field) driven by Nitrogen gas was applied on the other end of the sample.

The temperature was chosen from 340 K to 635 K, the cooling/heating rate was fixed to 2 K/min and AC field frequencies were 0.2, 0.4, 1, 4, 10, 20 Hz, respectively.

3. Results

3.1. DSC results of $Ti_{50}(Pd_{50-x}Cr_x)$ with x ranging from 4.0 to 5.0

DSC results of $Ti_{50}(Pd_{50-x}Cr_x)$ SMAs with x ranging from 4.0 to 5.0 are shown in Fig. 1 (b). The exothermal/endothermic peaks in these DSC curves and the thermal hysteresis associated with the transformation (> 13 K) suggest that all the $Ti_{50}(Pd_{50-x}Cr_x)$ samples undergo a normal first order martensitic transformation. It is shown that with increasing Cr concentration x, the start temperature of martensitic transformation (M_s), is reduced from 615 K of 4.0 Cr to 542 K of 5.0 Cr. Fig. 1 (c) plots the M_s as a function of Cr composition x. Such a composition dependence of transformation temperature is consistent with the reported phase diagram as shown in Fig. 1 (a). The corresponding transformation latent heat obtained from cooling processes decreases as well when Cr concentration x increases. However, there is an anomaly at x = 4.7, as shown in Fig. 1 (c). This phenomenon is in agreement with the ΔT results, in which the ΔT shows a minimum at x = 4.7, suggesting a possible composition crossover between two different transformations around x = 4.7 [22].

Table 1 summarizes the phase transformation properties of $Ti_{50}(Pd_{50-x}Cr_x)$ SMAs with x ranging from 4.0 to 5.0, including the martensitic transformation start and finish temperatures (M_s and M_f), the reverse transformation start and finish temperatures (A_s and A_f), thermal hysteresis ($\Delta T = \frac{1}{2}(A_s + A_f - M_s - M_f)$), and latent heat ($\Delta H$).

3.2. Damping capacities of $Ti_{50}(Pd_{50-x}Cr_x)$ with x ranging from 4.0 to 5.0

In this subsection, we investigated the damping capacities of all the

Table 1
The damping capacity and transformation properties of $Ti_{50}(Pd_{50-x}Cr_x)$ SMAs with x ranging from 4.0 to 5.0.

composition	M_s (K)	M_f (K)	A_s (K)	A_f (K)	ΔT (K)	ΔH (J/g)	Q^{-1} at M_s	Q^{-1} at 350 K	J (μm^2/N)
$Ti_{50}(Pd_{46.0}Cr_{4.0})$	615.30	597.54	620.55	637.22	22.47	19.39	0.058	0.053	65.14
$Ti_{50}(Pd_{45.8}Cr_{4.2})$	594.81	582.26	600.76	615.82	19.76	19.95	0.028	0.013	85.14
$Ti_{50}(Pd_{45.6}Cr_{4.4})$	588.41	568.00	582.96	607.20	16.88	18.07	0.024	0.011	104.30
$Ti_{50}(Pd_{45.5}Cr_{4.5})$	584.44	559.32	571.31	605.62	16.59	17.21	0.030	0.014	97.93
$Ti_{50}(Pd_{45.4}Cr_{4.6})$	578.05	549.44	562.41	591.54	13.23	14.62	0.041	0.020	110.54
$Ti_{50}(Pd_{45.3}Cr_{4.7})$	572.20	536.46	551.40	584.31	13.53	13.6	0.034	0.015	84.89
$Ti_{50}(Pd_{45.2}Cr_{4.8})$	560.02	542.45	555.84	575.87	14.62	14.11	0.029	0.013	120.73
$Ti_{50}(Pd_{45.0}Cr_{5.0})$	548.94	531.59	545.55	564.83	14.93	13.78	0.063	0.086	70.80

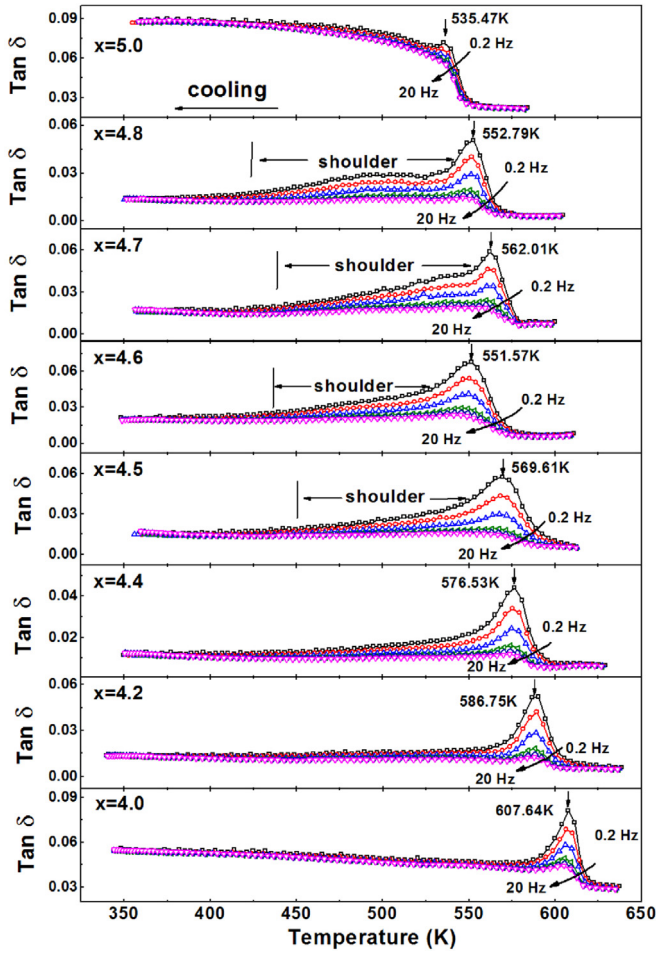

Fig. 2. Damping capacities of $Ti_{50}(Pd_{50-x}Cr_x)$ SMAs with x ranging from 4.0 to 5.0 as a function of temperature. They are obtained by dynamic mechanical analysis at different frequencies between 0.2 Hz and 20 Hz. The peak temperature defines the M_s and a damping capacity shoulder appears slightly below M_x for x = 4.8, 4.7, 4.6, and 4.5.

$Ti_{50}(Pd_{50-x}Cr_x)$ samples. Fig. 2 plots the damping capacity tanδ at different frequencies between 0.2 Hz and 20 Hz within the temperature range of 340 K–635 K. A sharp internal friction peak can be identified in every tanδ *vs.* temperature curve, as indicated by the arrows in Fig. 2. The peak temperature is where the martensitic transformation takes place. Obviously, the transformation temperature decreases monotonously with the increase of the Cr concentration x. The transformation temperature as a function of x is also plotted in Fig. 1 (c), and it is consistent with the DSC measurement.

It is noted that no frequency dispersion, *i.e.* the frequency dependence of transformation temperature, can be observed in the sharp damping peak, indicating that they are martensitic transformations. When Cr concentration is smaller than 4.5% (x< 4.5%), only the martensitic transformation damping peak is observed. When Cr concentration is large (x= 5.0%), a high damping plateau over a wide temperature range appears after the martensitic transformation damping peak, which can attribute to energy dissipation due to the twin boundary motion [6,7]. For Cr concentrations in between (4.5 %< x < 5.0%), it can be observed that the sharp damping peak has a "shoulder" on the low temperature side. It is more obvious at lower frequencies. Especially for x = 4.8%, the "shoulder" becomes into a broad relaxation-type damping peak, which lies slightly below the sharp internal friction peak. The shoulders can also be observed upon heating and they are not one-way effect.

It can be seen that the damping capacity in the martensitic state for $Ti_{50}(Pd_{45}Cr_5)$ is larger than that of $Ti_{50}(Pd_{46}Cr_4)$. Compared with 9 R martensite phase, the B19 martensite involves larger transformation strain and resulted low mobility of twin boundaries, which leads to the low damping capacity. Therefore, the $Ti_{50}(Pd_{45}Cr_5)$ alloy with B19 and 9 R phases shows higher damping capacity than that of $Ti_{50}(Pd_{46}Cr_4)$ alloy with B19 phase only. The damping capacity in the martensitic state increases upon cooling for the two terminal compositions (x = 4.0, 5.0). It is known that hydrogen always interacts with twin boundaries in TiPd and TiNi based alloys, leading to a "broad relaxation peak" after the martensitic transformation where martensite twins exist. Such a relaxation damping peak with high damping capacity normally locates around 300 K in TiPd-based alloys. Thus, the damping capacity in the martensitic state increases on cooling towards the twin boundary - hydrogen relaxation peak.

3.3. Storage compliance of $Ti_{50}(Pd_{50-x}Cr_x)$ with x ranging from 4.0 to 5.0

As the storage compliance is closely related with the damping capacities, we plot the storage compliance as a function of temperature for all the $Ti_{50}(Pd_{50-x}Cr_x)$ samples. The results are shown in Fig. 3 and the frequency range is between 0.2 Hz and 20 Hz. The storage compliance exhibits a discontinuity at the martensitic transformation temperature upon cooling. We define the inflection point in the storage compliance *vs.* temperature curve upon cooling as the M_s temperature, as indicated by the arrows in Fig. 3. The M_s temperature as a function of x is also plotted in Fig. 1 (c).

It can be seen that the storage compliance shows a little frequency dependent in both high temperature austenite and low temperature martensite phases, but much more frequency dependent during the martensitic transformation, which is the characteristic of normal martensitic transformations.

4. Discussion

4.1. The damping peak at the martensitic transformation temperature

The damping capacity peak during the martensitic phase transformation, especially measured at low frequencies (<10 Hz), is a results of hysteretic motion of phase fronts between austenite and martensite. The phase fronts are a result of the nucleation and growth of a new phase. Therefore, the low-frequency damping capacity at the

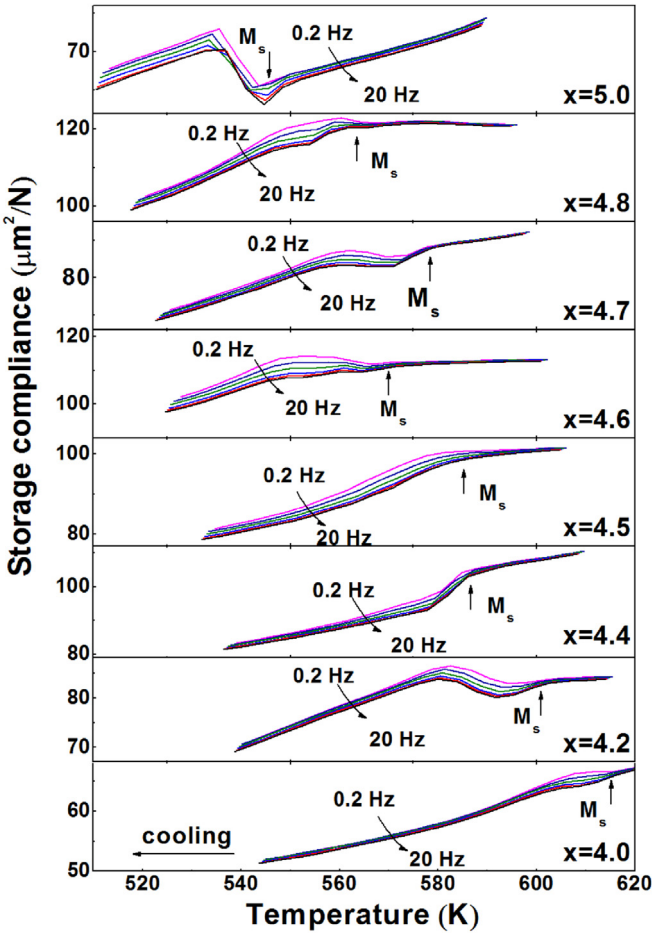

Fig. 3. Storage compliance of $Ti_{50}(Pd_{50-x}Cr_x)$ SMAs with x ranging from 4.0 to 5.0 as a function of temperature. They are obtained by dynamic mechanical analysis at different frequencies between 0.2 Hz and 20 Hz.

martensitic transformation is related to the volume fraction of transformed phase, the heating/cooling rate dT/dt and the measurement frequency f. The internal friction associated with the martensitic phase transformation can be expressed by Refs. [14,23],

$$Q^{-1} = \frac{\Delta\bar{J}}{\bar{J}}\frac{dM(T)}{dT}\left(\frac{dT}{dt}\right)^{p}\omega^{-l} \quad (1)$$

where $\Delta\bar{J}$ is the average change of the compliance due to the phase transformation, $\bar{J}$ is the average compliance of the material, $M(T)$ is the volume fraction that has transformed to a new phase at the temperature T, p and l are constants, and $\omega = 2\pi f$. Equation (1) shows that the internal friction is inversely proportional to the frequency. For the first approximation, the $\frac{dM(T)}{dT}\left(\frac{dT}{dt}\right)^{p}$ term can be considered as constant, as the heating/cooling rate dT/dt is fixed in our measurement. This explains the observation of the lower damping capacity at higher frequency.

For the ferroelectric transition in ceramics, the p and l in 1 are usually equal to one [14,23]. However, we found here in our alloys the l is equal to 0.5. Fig. 4 shows the damping capacity as a function of $\omega^{-0.5}$. A linear dependence of damping capacity on $\omega^{-0.5}$ can be observed in every $Ti_{50}(Pd_{50-x}Cr_x)$ samples. The R^2 values for all the linear relations are greater than 0.97, indicating a good linear correlation. Therefore, the damping capacity of $Ti_{50}(Pd_{50-x}Cr_x)$ ($4.0 \leqslant x \leqslant 5.0$) SMAs is inversely proportional to the square root of frequency, *i.e.,* $Q^{-1} \propto \omega^{-0.5}$. Wang et al. [24] and Zhang et al. [25] have shown that the parameter l in Equation (1) can be less than one in their models, especially for materials with elastic softening [14]. It is well known that there exists a

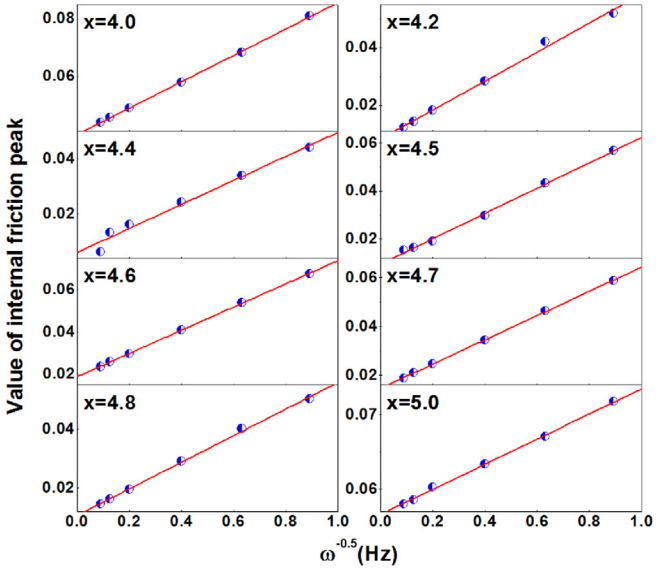

Fig. 4. The damping capacity at the martensitic transformation temperature as a function of $\omega^{-0.5}$ for $Ti_{50}(Pd_{50-x}Cr_x)$ alloys. The damping capacity is inversely proportional to the square root of frequency, *i.e.,* $Q^{-1} \propto \omega^{-0.5}$.

strong elastic softening before martensitic transformation in shape memory alloys. Thus our finding of $Q^{-1} \propto \omega^{-0.5}$ is reasonable and consistent with the models of Wang et al. [24] and Zhang et al. [25].

Besides the damping capacity, we also plot the storage compliance at the martensitic transformation as a function of $\omega^{-0.5}$. Fig. 5 shows the results and it can be seen that the storage compliance linearly depends on the $\omega^{-0.5}$ for all the samples. The storage compliance is inversely proportional to the square root of frequency, *i.e.,* $Q^{-1} \propto \omega^{-0.5}$, as well.

4.2. The damping shoulder at the compositional crossover region

As shown in Fig. 2, there is a broad damping capacity shoulder slightly below the martensitic transformation for every sample within the compositional crossover region (x = 4.8, 4.7, 4.6, and 4.5). Its damping capacity (at 1 Hz) is around 0.03 for these alloys and covers temperatures from 450 K to 550 K. Within such a temperature range,

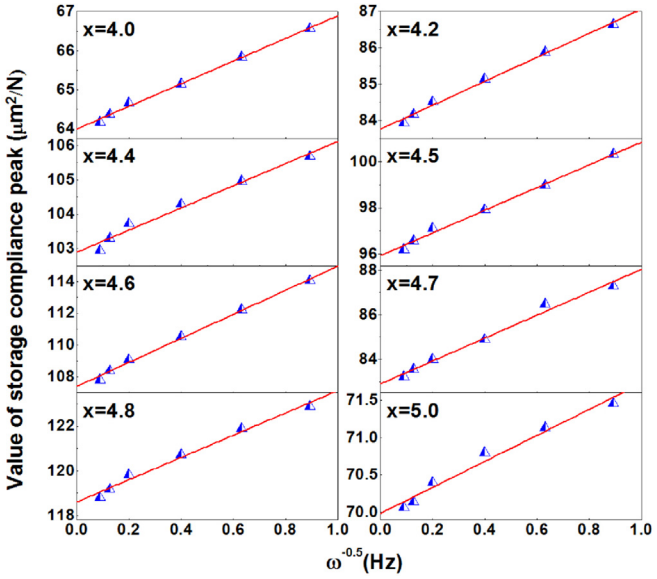

Fig. 5. The storage compliance at the martensitic transformation temperature as a function of $\omega^{-0.5}$ for $Ti_{50}(Pd_{50-x}Cr_x)$ alloys. The storage compliance is inversely proportional to the square root of frequency, *i.e.,* $Q^{-1} \propto \omega^{-0.5}$.

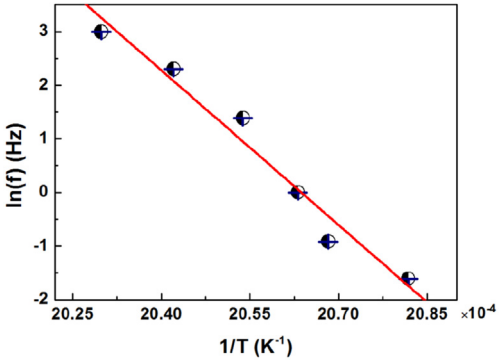

Fig. 6. ln(f) versus 1/T plot of the broad damping peak in $Ti_{50}(Pd_{45.2}Cr_{4.8})$ fits the Arrhenius relationship (where T is the peak position corresponding to each frequency), indicating that it is a relaxation-type damping peak. Error bar is from picking up the peak temperature for 5 times.

the storage compliance shows no anomaly, indicating that no structure change or transformation occurs [26]. Thus, these damping shoulders or peaks are most likely of relaxation type.

It can be seen from Fig. 2 that the broad damping capacity shoulder shows frequency dispersion in every sample within the compositional crossover region. It appears in $Ti_{50}(Pd_{45.2}Cr_{4.8})$ as a broad peak, and we will discuss this one in the following. The peak temperature shifts to high temperature with increasing frequency. The peak temperature versus frequency relation follows the Arrhenius relation, $\omega = \omega_0 e^{-\frac{E_a}{k_B T}}$, as shown in Fig. 6). This indicates that this damping peak is of a relaxational type.

It has been reported that there is a relaxational peak in martensite phase of TiPd-based alloys [6,7]. And it is considered that the twin boundary-hydrogen interaction can be one reasonable origin for that peak [6,7]. However, the hydrogen related damping peak always locates around 300 K, which is well below the temperature of our damping shoulder. And it is noted that all the damping shoulders occur only at the compositional crossover region, not in the two side compositions. At the compositional crossover region, there exist different interfaces among three phases including B2, B19 and 9 R. Thus we considered that damping peak of martensitic transformation is due to the interface between austenite and martensite and the damping shoulder is probably as a result of the hysteretic motion of interface between two martensitic phases, *i.e.,* B19 and 9 R, under external stress. But the detailed mechanism for the damping shoulder still remains covered.

4.3. Damping behaviors as a function of Cr concentration

In this section, the dependence of damping capacity on the Cr concentration is investigated and the underlying mechanism is discussed. Fig. 7 (a) plots the damping capacity at the martensitic transformation temperature of different frequencies as a function of Cr concentration *x*. It can be found that the damping capacity is smaller within the compositional crossover region, compared with samples at both sides. An opposite tendency arises in the storage compliance at the martensitic transformation *vs.* Cr concentration curves, as shown in Fig. 7 (b).

We tried to connect the composition dependence of damping capacity and storage compliance with the possible microstructure. The small damping capacity and large storage compliance appear within the compositional crossover region between two different martensitic transformations (B2-B19 and B2-9 R, respectively). Thus the crossover region corresponds a phase boundary between B19 and 9 R martensites. And within the compositional crossover region, different martensite phases (B19 and 9 R) can be degenerate in energy. The TEM observations by Enami et al. have shown that B19 and 9 R phases indeed coexist

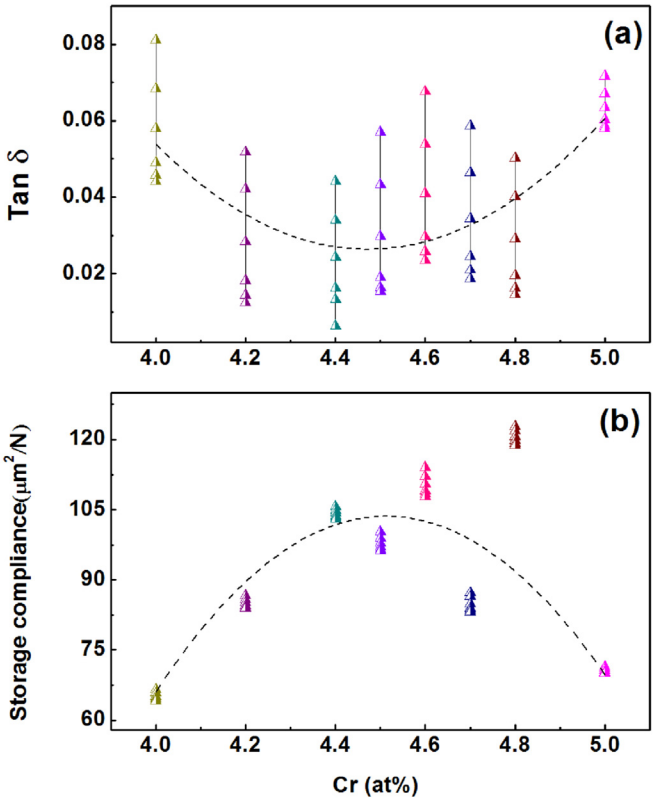

Fig. 7. (a) the damping capacity at the martensitic transformation temperature of different frequencies and (b) the storage compliance at the martensitic transformation temperature of different frequencies as a function of Cr concentration *x* in $Ti_{50}(Pd_{50-x}Cr_x)$ alloys. Dashed lines are guide eyes.

at the crossover region of defect doped Ti-Pd based SMAs, which supports our understanding here in spite of the different dopants [27].

Due to the structural instability at the phase boundary, the mechanical perturbation may result in easy switching between different phases, *i.e.*, the energy barriers associated with the interfaces of martensite B19 and 9 R are rather low. Consequently, less energies are dissipated during interface motion, resulting in the smaller damping capacity and larger compliance within the compositional crossover region.

5. Summary

The damping behavior of $Ti_{50}(Pd_{50-x}Cr_x)$ was systematically investigated, the main results and conclusions are as follows:

- The damping capacity of $Ti_{50}(Pd_{50-x}Cr_x)$ ($4.0 \leqslant x \leqslant 5.0$) SMAs was found to be inversely proportional to the square root of frequency, *i.e.,* $Q^{-1} \propto \omega^{-0.5}$.
- An internal friction shoulder was found slightly below the martensitic transformation damping peak within the compositional crossover region ($4.5 \leqslant x \leqslant 4.8$). The relaxation peak may be ascribed to the hysteretic motion of interface between two coexisted phases.
- The damping capacity of martensitic transformation was found to be smaller within the compositional crossover region ($4.5 \leqslant x \leqslant 4.8$) than that of composition of both sides ($x = 4.0$ and $x = 5.0$). While the storage compliance shows the opposite tendency.

Acknowledgements

The authors gratefully acknowledge the support of National Natural Science Foundation of China (Grant Nos. 51571156, 51671157,

51320105014, 51621063, 51431007, and 51201126), and Program for Changjiaing Scholars and Innovative Research Team in University (IRT13034).

References

[1] D. James, High damping metals for engineering applications, Mater. Sci. Eng 4 (1969) 1–8.
[2] I.G. Ritchie, Z.L. Pan, High-damping metals and alloys, Metall. Trans. A 22 (1991) 607–616.
[3] R. Schaller, G. Fantozzi, G. Gremaud, Mechanical Spectroscopy Q[-][1] 2001 with Applications to Materials Science, Trans Tech Publications LTD, 2001.
[4] F. Yin, S. Iwasaki, D. Ping, K. Nagai, Snoek-type high-damping alloys realized in β-Ti alloys with high oxygen solid solution, Adv. Mater. 18 (2006) 1541–1544.
[5] J.S. Juan, M.L. No, C.A. Schuh, Nanoscale shape-memory alloys for ultrahigh mechanical damping, Nat. Nanotechnol. 4 (2009) 415–419.
[6] Y. Zhou, G. Fan, D. Xue, X. Ding, K. Otsuka, J. Sun, X. Ren, High damping capacity in a wide ambient-temperature range in hydrogen-doped and hydrogen-free Ti–45Pd–5Cr martensitic alloy, Scripta Mater. 61 (2009) 805–808.
[7] D. Xue, Y. Zhou, X. Ding, K. Otsuka, T. Lookman, J. Sun, X. Ren, Ambient-temperature high damping capacity in TiPd-based martensitic alloys, Mater. Sci. Eng. A 632 (2015) 110–119.
[8] G. Mazzolai, Recent progresses in the understanding of the elastic and anelastic properties of H-free, H-doped and H-contaminated NiTi based alloys, AIP Adv. 1 (2011) 040701.
[9] X. Liao, Y. Wang, G. Fan, E. Liu, J. Shang, S. Yang, H. Luo, X. Song, X. Ren, K. Otsuka, High damping capacity of a Ni-Cu-Mn-Ga alloy in wide ambient-temperature range, J. Alloys. Compd. 695 (2017) 2400–2405.
[10] J.V. Humbeeck, Damping capacity of thermoelastic martensite in shape memory alloys, J. Alloys. Compd. 355 (2003) 58–64.
[11] K. Otsuka, C.M. Wayman, Shape Memory Materials, Cambridge university press, 1999.
[12] J.S. Juan, M. Nó, Damping behavior during martensitic transformation in shape memory alloys, J. Alloys. Compd. 355 (2003) 65–71.
[13] E.K.H. Salje, H. Zhang, H. Idrissi, D. Schryvers, M.A. Carpenter, X. Moya, A. Planes, Mechanical resonance of the austenite/martensite interface and the pinning of the martensitic microstructures by dislocations in $Cu_{74.08}Al_{23.13}Be_{2.79}$, Phys. Rev. B 80 (2009) 134114.
[14] R.B. Pérez-Sáez, V. Recarte, M.L. Nó, J. San Juan, Anelastic contributions and transformed volume fraction during thermoelastic martensitic transformations, Phys. Rev. B 57 (1998) 5684–5692.
[15] I. Yoshida, D. Monma, K. Iino, T. Ono, K. Otsuka, M. Asai, Internal friction of Ti–Ni–Cu ternary shape memory alloys, Mater. Sci. Eng., A 370 (2004) 444–448.
[16] F. Mazzolai, A. Biscarini, B. Coluzzi, G. Mazzolai, E. Villa, A. Tuissi, Low-frequency internal friction of hydrogen-free and hydrogen-doped NiTi alloys, Acta Mater. 55 (2007) 4243–4252.
[17] Z. Zhao, X. Ding, T. Lookman, J. Sun, E.K.H. Salje, Mechanical loss in multiferroic materials at high frequencies: friction and the evolution of ferroelastic microstructures, Adv. Mater. 25 (2013) 3244–3248.
[18] G. Fan, Y. Zhou, K. Otsuka, X. Ren, K. Nakamura, T. Ohba, T. Suzuki, I. Yoshida, F. Yin, Effects of frequency, composition, hydrogen and twin boundary density on the internal friction of $Ti_{50}Ni_{50x}Cu_x$ shape memory alloys, Acta Mater. 54 (2006) 5221–5229.
[19] G. Fan, Y. Zhou, K. Otsuka, X. Ren, Ultrahigh damping in R-phase state of Ti–Ni–Fe alloy, Appl. Phys. Lett. 89 (2006) 161902.
[20] K. Enami, K. Hori, J. Takahashi, Martensitic transformation in TiPd-Cr alloys, ISIJ Int. 29 (1989) 430–437.
[21] Y. Zhou, D. Xue, X. Ding, K. Otsuka, J. Sun, X. Ren, High temperature strain glass transition in defect doped Ti–Pd martensitic alloys, Phys. Status Solidi (b) 251 (2014) 2027–2033.
[22] D. Xue, R. Yuan, Y. Zhou, D. Xue, T. Lookman, G. Zhang, X. Ding, J. Sun, Design of high temperature Ti-Pd-Cr shape memory alloys with small thermal hysteresis, Sci. Rep. 6 (2016) 28244 EP.
[23] F. Yan, P. Bao, J. Zhu, Y. Wang, H.L.W. Chan, C.L. Choy, Phase transitions in Pb$(Mg_{1/3}Nb_{2/3})O_3$–$PbTiO_3$ studied by low-frequency internal friction measurement, J. Am. Ceram. Soc. 90 (2007) 3167–3170.
[24] Y. Wang, C. Xiaohua, S. Huimin, T.S. Ke (Ed.), Proceedings of the I.C.I.F.U.A.S.-9, Pergamon, New York, 1990.
[25] J.X. Zhang, P.C.W. Fung, W.G. Zeng, Dissipation function of the first-order phase transformation in solids via internal-friction measurements, Phys. Rev. B 52 (1995) 268–277.
[26] Y. Zhou, D. Xue, X. Ding, K. Otsuka, J. Sun, X. Ren, High temperature strain glass in $Ti_{50}(Pd_{50x}Cr_x)$ alloy and the associated shape memory effect and superelasticity, Appl. Phys. Lett. 95 (2009) 151906.
[27] K. Enami, Y. Nakagawa, 9R martensite in the Ti-Pd-Fe alloys, Proc. ICOMAT (1992) 521–526.